Published as: *Nature*. ; 483(7387): 47–52.

Gain control by layer six in cortical circuits of vision

Shawn R. Olsen[1,2], **Dante Bortone**[1,2], **Hillel Adesnik**, and **Massimo Scanziani**[1]

[1]Howard Hughes Medical Institute, Center for Neural Circuits and Behavior, Neurobiology Section and Department of Neuroscience, University of California San Diego, La Jolla, California 92093-0634, USA

Abstract

Upon entering the cerebral cortex sensory information spreads through six different horizontal neuronal layers that are interconnected by vertical axonal projections. It is believed that through these projections layers can influence each other's response to sensory stimuli, yet the specific role played by each layer in cortical processing is still poorly understood. Here we show that layer 6 in the primary visual cortex of the mouse plays a crucial role in controlling the gain of visually evoked activity in neurons of the upper layers without, however, changing their tuning to orientation. This gain modulation results from the coordinated action of layer 6 projections to superficial layers and deep projections to the thalamus, with a substantial role of the former circuit. This study thus establishes L6 as a major mediator of cortical gain modulation and suggests it could be a node through which convergent inputs from several brain areas can regulate the earliest steps of cortical visual processing.

Primary sensory areas in the cerebral cortex are composed of a stack of six neuronal layers[1]. Anatomical and physiological data indicate that these layers are interconnected via vertical excitatory axons[2–6], suggesting that sensory processing in any given layer may be modulated by activity in several other layers. To date, however, the exact contribution of each layer to cortical processing is unclear.

Here we address the role of layer 6 (L6) in mouse visual cortex, whose excitatory neurons not only project to more superficial layers but also to the primary sensory thalamic nuclei[3, 7–11], the main source of sensory input to the cortex (Fig. 1a). L6 may thus influence cortical sensory responses directly via intra-cortical projections and indirectly via cortico-thalamic projections. Cortico-thalamic projections were reported to be both suppressive and facilitatory on thalamic activity, depending on the precise alignment between L6 and thalamic neurons (for reviews see refs[12–16]). In contrast, how sensory responses in cortex are affected by L6 activity has remained largely unexplored[17, 18]. Furthermore, the relative contribution of intra-cortical versus cortico-thalamic projections in modulating cortical responses is currently unknown. The paucity of information is due to the lack of experimental tools for selectively manipulating activity in L6 without directly perturbing other cortical layers.

Correspondence: Massimo Scanziani, Neurobiology Section, mail code 0634, University of California, San Diego, 9500 Gilman Drive, La Jolla, CA 92093-0634, massimo@biomail.ucsd.edu. Shawn Olsen, Neurobiology Section, mail code 0634, University of California, San Diego, 9500 Gilman Drive, La Jolla, CA 92093-0634, srolsen@ucsd.edu.
[2]these two authors contributed equally

Author Contributions

H.A. performed the initial physiological characterization of the NTSR1-Cre expression system with optogenetic tools. H.A also developed the *in vivo* awake recording preparation on the treadmill. S.R.O. performed all *in vivo* recordings. D.B. performed all *in vitro* recordings and anatomical reconstructions. S.R.O. and M.S. designed the study. M.S. wrote the paper.

To control the activity of L6 we took advantage of a Cre-recombinase Bac transgenic mouse-line reported to selectively label L6 neurons (NTSR1-Cre GN220)[19]. In the forebrain of these mice Cre-expression was restricted to excitatory L6 neurons of the cerebral cortex (Fig. 1b and Supplementary Fig. 1). In primary visual cortex (V1) these neurons represented ~65% of the L6 excitatory neuronal population and, consistent with classification of L6 neurons in this region[1], could be subdivided into two morphologically distinct categories: those whose apical dendrites ended in L4 (32%) and those that extended to L1 (68%) (Fig. 1b and Supplementary Fig. 1g,h). Furthermore, consistent with the cortico-thalamic projections originating from L6 in V1[8], Cre-expresssing neurons projected to the dorsolateral geniculate nucleus (dLGN; the primary thalamic visual nucleus) and the nucleus reticularis thalami (nRT; the main thalamic inhibitory nucleus) (Fig. 1b and Supplementary Fig. 1d,e). Thirty-five percent of L6 excitatory neurons in V1 did not express Cre and these were morphologically distinct from the Cre expressing population (Supplementary Fig. 1g).

To manipulate the activity of L6 neurons we conditionally expressed the light-sensitive cation channel channelrhodopsin 2 (ChR2)[20, 21] in V1 using viral injection into NTSR1-Cre mice (Supplemental Fig. 2a). A linear multichannel probe recorded the spiking activity of neuorns located across the vertical depth of cortex. Light-emitting diode (LED) illumination of the cortical surface for 500 ms with blue light (470 nm) increased the activity of L6 neurons in V1 of anesthetized animals (Fig. 1c–e and Supplemental Fig. 2b). This increase was not due to direct stimulation of the retina by the LED since it was absent in uninjected animals (Supplemental Fig. 2g).

How does activation of L6 impact visually evoked activity in other layers? We presented drifting gratings and alternated control trials (visual stimulus only) with trials in which L6 was photo-stimulated (Fig. 1c). Strikingly, photo-stimulation of L6 rapidly and reversibly suppressed visually evoked multiunit activity throughout the depth of the cortex (Fig. 1d; L6 photo-stimulation also reduced spontaneous activity; Supplemental Fig. 3d,e). This effect was absent in uninjected animals (Supplemental Fig. 2g). The suppressive action of L6 was similar across layers 2/3, 4 and 5 and was monotonic (Fig. 1e,f): that is, increasing L6 activity by increasing illumination intensity progressively suppressed visual responses, eventually abolishing nearly all evoked activity (strongest illumination reduced activity by 81±5%, 84±3%, and 84±3% for L2/3, L4, and L5, respectively; $p < 10^{-5}$). Because multiunit activity is dominated by neurons with high firing frequencies, we determined the effect of L6 photo-stimulation on isolated single units whose average visually evoked firing rate varied over a 20-fold range. Isolated units were suppressed by L6 photo-stimulation (Fig. 1g), irrespective of their firing rates (Fig. 1h; 91.1% of units were suppressed and 7.8% were facilitated; all facilitated units were fast spiking, putative inhibitory cells (Supplmental Fig. 4a–d), see methods). Furthermore, as for multiunit activity, L6 photo-stimulation monotonically suppressed single units (Fig. 1i,j; strongest illumination reduced activity by 91±4%, 93±2%, and 92±2% for L2/3, L4, and L5, respectively; $p < 10^{-9}$). Thus, these data show that stimulation of L6 excitatory neurons suppresses visually evoked responses in layers 2/3, 4 and 5 of V1.

Like in other mammals, neurons in mouse V1 differentially respond to gratings of different orientations [22, 23]. Does L6 stimulation affect the orientation tuning of V1 neurons? We generated tuning curves by presenting gratings drifting in 8–12 different directions and alternated control trials with trials where L6 was photo-stimulated (Fig. 2a,b). We used a low LED intensity so as to partially silence cortical visual responses, and considered units that were suppressed by between 10% and 75% (average suppression 42±3%, n = 55). Tuning curves of individual, isolated units were averaged into a population tuning curve (Fig. 2b,d; see methods). Remarkably, photo-stimulation of L6 resulted in the precise scaling of the tuning curve, that is it reduced visually evoked responses by a similar fraction

irrespective of presented orientation. This is clearly illustrated by plotting the normalized firing rates of the population tuning curve under control versus L6 photo-stimulation conditions (Fig. 2e). The data-points are well-fit with a line whose slope is 0.56 and intercepts the y-axis close to the origin. Thus, photo-stimulation of L6 did not affect preferred orientation, tuning width, or the orientation selectivity index (OSI) of cortical neurons throughout layers 2/3, 4 and 5 (Fig. 2c; for L2/3, L4, and L5, respectively, the mean change in preferred orientation was 3±3° ($p = 0.22$), 0±5° ($p = 0.9$), and −4±5° ($p = 0.48$), mean change in tuning width was −1±4° ($p = 0.8$), 6±4° ($p = 0.15$), and −6±6° ($p = 0.3$), and mean change in OSI was −0.09±0.07 ($p = 0.23$), 0.7±0.04 ($p = 0.14$), −0.06±0.05 ($p = 0.22$)). L6 photo-stimulation also resulted in a scaling of V1 responses to stimuli of increasing contrast (the contrast response function; Supplemental Fig. 5b). These data demonstrate that in primary visual cortex L6 selectively controls the gain of cortical responses to visual stimuli.

A potential concern in stimulating L6 with ChR2 is that the spatially uniform activation and the temporal pattern generated in L6 neurons may differ from visually evoked activity patterns, and thus physiological activity of L6 neurons may impact cortical activity in a manner different than L6 photo-stimulation. Furthermore, anesthesia may affect the impact of L6 on cortical responses to sensory stimuli. To address these issues, we optogenetically suppressed visually evoked activity in L6 in awake animals and determined the resulting effect on more superficial layers (Supplemental Fig. 6). Animals were head-fixed but otherwise kept unrestrained on a passive circular treadmill (see methods). L6 activity was suppressed using conditionally-expressed light-sensitive hyperpolarizing opsins archeorhodopsin[24] (Arch) and halorhodopsin3.0[25] (NpHR3.0). LED illumination with amber light (590 nm), while reducing visual evoked L6 activity by ~30% (Supplemental Fig. 6e), significantly facilitated visual responses of isolated units throughout the other layers (Fig. 2f,g and Supplemental Fig. 6). The facilitation was not due to direct LED illumination of the retina since it was absent in uninjected animals (Supplemental Fig. 6f). Thus, suppression of L6 facilitates visually evoked activity in layers 2/3, 4 and 5, indicating that even physiologically generated L6 activity exerts a suppressive action onto these layers. Furthermore suppression of L6 resulted in the precise scaling of the tuning curve (for the tuning curve analysis we considered units that were facilitated by at least 10% (average facilitation 41±7%, $n = 52$)). The plot of normalized firing rates under control versus L6 photo-suppression conditions was well-fit by a line whose slope is 1.4 and intercepts the y-axis very close to the origin (Fig. 2j). Accordingly, suppressing L6, did not affect preferred orientation, tuning width, or orientation selectivity (Fig. 2h; for L2/3, L4, and L5, respectively, the mean change in preferred orientation was 2±3° ($p = 0.41$), 0±2° ($p = 0.95$), and −4±4° ($p = 0.35$) degrees, mean change in tuning width was −2±4° ($p = 0.68$), 0±3° ($p = 0.94$), and −1±4° ($p = 0.77$) degrees, and mean change in OSI was −0.01±0.03 ($p = 0.22$), 0.02±0.02 ($p = 0.50$), −0.03±0.03 ($p = 0.22$)). Taken together, these results demonstrate that visually-driven L6 activity in awake animals controls the gain of cortical responses to visual stimuli.

What circuit(s) mediate the suppression exerted by L6 on cortical activity? On one hand, L6 neurons project to the thalamus, where they can influence visually generated activity before it even reaches the cortex. On the other hand, L6 neurons also project to more superficial layers where they could directly modulate cortical activity. We addressed the impact of both projections. We performed extracellular recordings from the dLGN while photo-stimulating L6 in V1 (Fig. 3a). dLGN relay neurons were identified based on their visual response properties and characteristic firing pattern (Supplementary Fig. 7d). Photo-stimulation of L6 led to a rapid, reversible and monotonic reduction of visually evoked activity in dLGN relay neurons (Fig. 3b,c; strongest illumination: 76±4% reduction; $p<10^{-10}$, $n = 32$), without, however, markedly modifying their firing mode (burst prevalence: 12±6% in control; 6±3%

after reducing dLGN activity by 30% with L6 photo-stimulation, p = 0.08; Supplemental Fig. 7e,f). This indicates that L6 stimulation suppresses dLGN activity. To test whether visually evoked activity in L6 ongoingly suppresses dLGN activity we silenced the cortex optogenetically (by photo-stimulating parvalbumin-expressing (PV) inhibitory neurons in V1 with ChR2; see methods and Supplementary Fig. 8). Consistent with the suppressive action of L6 stimulation on dLGN, silencing the cortex strongly facilitated dLGN activity (Fig. 3d–f; average facilitation 87+/−25% (p = 0.002, n = 18)). *In vitro* recordings demonstrated that the suppressive action of L6 was due to the generation of disynaptic inhibition onto dLGN relay neurons, at least in part via the recruitment of nRT inhibitory neurons (and possibly through the recruitment of local inhibitory neurons in dLGN[26]) (Supplemental Fig. 9). Thus, these results reveal that L6 can effectively suppress visual responses in the dLGN.

If L6 suppresses cortical visual responses indirectly, by suppressing the dLGN, this suppression should precede V1 suppression by a few milliseconds. We tested this prediction by performing simultaneous recordings from both dLGN and V1 and compared the onset of suppression in these two structures upon L6 photo-stimulation (Fig. 3g). Surprisingly, cortical suppression *preceded* dLGN suppression by a few ms (Fig. 3h). This result suggests that L6 activity may suppress cortical visual responses through an alternative circuit. Because L6 neurons send axons to the upper layers of cortex we tested whether these projections can suppress cortical activity independently of the cortico-thalamic projections. For this, we performed *in vitro* whole cell recordings from neurons in L2/3, 4, 5 and 6 in coronal slices of V1 (Fig. 4a), a slicing plane disconnects V1 from dLGN.

Photo-stimulation of L6 *in vitro* generated both excitatory and inhibitory postsynaptic currents (EPSCs and IPSC, respectively) onto L2/3, 4, 5 and 6 pyramidal cells (L6 recordings included only those pyramidal cells not expressing ChR2) (Fig. 4b). IPSCs were of disynaptic (or polysynapyic) origin since they were entirely blocked by glutamatergic antagonists (Supplemental Fig.10b). Furthermore, the activity pattern generated by L6 photo-stimulation was similar to the activity pattern generated *in vivo* (Supplementary Fig. 2b,h). IPSCs were larger than EPSCs, despite the fact that both currents were recorded with a similar driving force (IPSCs were recorded near the reversal potential for EPSCs and vice versa). Indeed, excitatory charge accounted for only 10 % or less of the total charge, depending on layer (Fig. 4c) or sublayer (Supplemental Fig. 10c,d). These results demonstrate that V1 contains the necessary circuitry for L6 to generate disynaptic inhibition onto layers 2/3, 4, 5 and onto itself.

To determine whether, through these disynaptic IPSCs, L6 can suppress neuronal spiking across L2/3, 4, 5 and 6, we performed current clamp recordings in the perforated patch configuration (to preserve the intracellular ionic composition) and triggered spiking by injecting depolarizing current pulses. Photo-stimulation of L6 significantly suppressed firing of pyramidal cells across all layers (Fig. 4d). To rule out the possibility that this suppression resulted from uniformly activating large portions of L6 we restricted the area of activation to a small spot of approximately 100 μm in diameter while recording from a L5 neuron, as above (Fig. 4f). Even when activating a restricted area of L6, the firing of L5 neurons was robustly suppressed (Fig. 4g). The suppression was maximal when L6 photo-stimulation was aligned with the recorded L5 neuron along the cortical radial axis, and decreased progressively as the photo-stimulation spot was translated tangentially (Fig. 4g,h). These results demonstrate that V1 can efficiently suppress activity in layers 2/3, 4, 5 and 6 in the absence of thalamus.

Taken together, these results indicate that L6 can modulate cortical responses to visual stimuli through two independent circuits: indirectly, via the cortico-thalamic circuit and

directly through the intra-cortical circuit. Does one of these two circuits play a dominant role? We addressed this by asking how much of the V1 suppression is predicted by dLGN suppression. We first established the transfer function between dLGN and V1. For this we performed simultaneous *in vivo* recordings from these two structures, while presenting full-field drifting gratings of varying contrasts in order to obtain contrast response functions for the dLGN and V1 (Fig. 5a,b). By plotting dLGN versus V1 activity at each contrast we obtained the transfer function from dLGN to V1,which provides the response of V1 to various levels of dLGN activity (Fig. 5c). Finally, we presented the strongest contrast and photo-stimulated L6 to reduce dLGN activity, while simultaneously monitoring V1 activity. We reasoned that if the ensuing reduction of V1 activity matches the reduction predicted by the transfer function, the modulation of cortical responses by L6 is mainly due to dLGN suppression via the cortico-thalamic circuit. If, on the other hand, the reduction in V1 activity exceeds that predicted by the transfer function, the additional reduction can be attributed to the intra-cortical circuit. We reduced dLGN activity by ~10%, 20% and 50% via activation of L6 with three progressively stronger illuminations (Fig 5d). Strikingly, even the smallest reduction in dLGN activity (10%) was accompanied by a reduction in V1 activity that largely exceeded that predicted by the transfer function (Fig. 5e). Furthermore, a 50% suppression of dLGN activity was accompanied by a complete suppression of visual evoked activity in V1. In this experiment a large fraction of V1 suppression (73% averaged over 5 LED levels) exceeded the transfer function prediction and must thus be attributed to the intra-cortical circuit (average intra-cortical component over all experiments 73±5%, n = 5; Fig. 5f). Furthermore, given the relatively minor effects on the prevalence of burst firing in dLGN neurons (see above and Supplemental Fig. 7f), it is unlikely that the L6 photo-stimulation substantially affected the transfer function. These results indicate that L6 suppresses cortical responses to visual stimuli in large part through intra-cortical circuits.

Taken together, this study shows that L6 modulates visually evoked activity across layers 2/3, 4 and 5. This modulation occurs ongoingly through visually driven L6 activity, as shown in awake animals and does not affect orientation tuning indicating that L6 selectively controls the gain of cortical visual responses. Finally, despite suppression of the dLGN, cortical gain control by L6 is executed largely by intra-cortical circuits.

Response gain modulation is a fundamental cortical operation[27], crucially involved in sensory representation and sensorimotor integration. For example, visual responses in parietal cortex are gain modulated by gaze direction[28]. Furthmore, gain modulation may underlie the effects of attention on cortical responses to visual stimuli[29, 30]. The neuronal circuits that implement this operation have, however, remained largely unknown. Identifying L6 as a contributor to cortical response gain modulation is an important step in dissecting the specific functions of distinct circuits in cortical processing. The suppressive action of L6 described here markedly differs from the facilitatory impact of other layers on cortical activity[3, 31, 32] (e.g. L2/3 facilitates L5[32]) and points towards a very distinct function of different layers in sensory processing. The cortical GABAergic interneuron subtype(s) [33, 34] that are recruited by L6 activity and mediate the reported suppressive effect remain to be identified, yet may include fast spiking neurons (Supplemental Fig. 4). While the exact synaptic mechanisms underlying gain control by L6 will have to be elucidated, either a proportional change in excitation and inhibition[35, 36] or the modulation of only one of the two opposing conductances[37] may underlie the operation. The columnar organization of L6 pyramidal cell projections to more superficial layers[10] ensure that L6 mediated suppression is restricted to the cortical domains directly above the activated L6 region (Fig. 4g–h). This topographic organization could allow the cortex to differentially modulate the gain of the response of V1 to stimuli located in distinct regions of visual space.

L6 has been suggested to contribute to “end-inhibition”, the suppression of cortical responses by bars above a given size[17]. The powerful inhibitory currents generated by L6 onto more superficial pyramidal cells may represent the underlying cellular mechanism.

Previous studies addressing the role of cortico-thalamic feedback projections through focal pharmacological perturbation of L6 neurons have typically reported a facilitation of functionally or topographically aligned thalamic neurons overlaid by broader surround suppression[16], resulting in changes to both spatial and temporal tuning properties of these neurons[15, 38–41]. Our data obtained using full-field visual stimulation are consistent with this model, where spatial summation of individual inhibitory surrounds will result in a net suppressive effect of the cortico-thalamic feedback projection. Future studies combining optogenetic approaches with focal stimulation of visual space will reveal how fine-scale cortico-thalamic circuits[39, 42] interact with intra-cortical L6 circuits to influence visual processing in the cortex.

L6 in V1 receives convergent inputs from a variety of brain regions, including higher cortical areas[43] as well as thalamus[11]. These various brain regions could thus influence, through L6, the gain of visual responses during the very initial steps of visual cortical processing.

Methods

All procedures were conducted in accordance with the National Institutes of Health guidelines and with the approval of the Committee on Animal Care at UCSD.

Animals

We used the following mouse lines: NTSR1-Cre (Strain name: B6.FVB(Cg)-Tg(Ntsr1-cre)GN220Gsat/Mmcd; Stock number: 030648-UCD) generated by the GENSAT project[19] and acquired from the Mutant Mouse Regional Resource Centers; tdTomato reporter (Jax: 007908); GAD67-GFP (Δneo); PV-Cre (Silvia Arber).

Viral injections

AAV viruses for Channelrhodopsin-2 (ChR2) and Archaerhodopsin (Arch) were acquired from the U. Penn Viral Vector Core: AAV2/1.CAGGS.flex.ChR2.tdTomato.SV40 (Addgene 18917) and AAV2/9.flex.CBA.Arch-GFP.W.SV40 (Addgene 22222). An AAV virus (AAV2/9) for Halorhodopsin3.0 (NpHR3.0) was produced at the Salk Viral Vector Core. The NpHR3.0 plasmid (pAAV-Ef1a-DIO-eNpHR 3.0-EYFP) was provided by Karl Diesseroth.

Viruses were loaded in a beveled sharp micropipette mounted on a Nanoject II (Drumond) or a micropump injector (UMP-3 WPI), attached to a micromanipulator. ChR2 virus was injected into newborn (P0–P2) pups anesthestized on ice and secured into a molded platform. Three 20 nL boli of virus was injected at each of 3 x–y locations and 2 depths (500 and 650 μm) within primary visual cortex (V1).

Arch was injected in combination with NpHR3.0 in juvenile (1–2 month) mice anethestized with 2.5% isoflurane and placed into a stereotactic frame (Knopf). The exposed skull overlying V1 was thinned in 3 locations with a dental drill (Foredom; 300 μm bur (Gesswein)) and a hole was made with a needle (25 gauge) at each location to permit insertion of the injection pipette A volume of 150 nL of virus was injected at a rate of 20 nL/min at each of the three locations and at 2 depths (900 and 700 μm). The scalp was then sutured and the mouse injected subcutaneously with 0.1 mg/kg buprenorphine. *In vivo* recordings were made 1–2 months following viral injection.

Slice preparation

Mice were anesthetized with ketamine and xylazine (100 mg/kg and 10 mg/kg, respectively), perfused transcardially with cold sucrose solution (in mM: NaCl 83, KCl 2.5, $MgSO_4$ 3.3, NaH_2PO_4 1, $NaHCO_3$ 26.2, D-Glucose 22, Sucrose 72, $CaCl_2$ 0.5 bubbled with 95% O_2 5% CO_2), decapitated and the visual cortex cut into 300–400 μm coronal sections in cold sucrose solution. Thalamic slices were cut 45° off the coronal plane to maintain connections between nRT and dLGN. Slices were incubated in sucrose solution in a submerged chamber at 34°C for 30 minutes and then at room temperature until used for recordings.

In vitro recordings

Whole cell recordings were done at 32°C in artificial cerebrospinal fluid (in mM: NaCl 119, KCl 2.5, NaH_2PO_4 1.3, $NaHCO_3$ 26, D-Glucose 20, $MgCl_2$ 1.3, $CaCl_2$ 2.5; mOsm 305; bubbled with 95% O_2 5% CO_2). Excitatory and inhibitory synaptic currents were recorded using a Cesium-based internal solution (in mM: $CsMeSO_4$ 115, NaCl 4, HEPES 10, Na_3GTP 0.3, MgATP 4, EGTA 0.3, QX-314-Cl 2.5, BAPTA(5Cs) 10; adjusted to pH 7.4 with CsOH; mOsm 295; 3–5 MOhm pipette resistance). Voltage clamp recordings were not considered if the series resistance exceeded 20MOhm or varied by more than 10%. Typically 2–4 neurons were recorded from simultaneously. Cell attached recordings and biocytin fills were done with a potassium based internal solution (in mM: K-gluconate 150, $MgCl_2$ 1.5, HEPES 5, EGTA 1.1, Phosphocreatine 10; adjusted to pH 7.4 with KOH; mOsm 295). Perforated patch recordings were done using potassium based internal and 10μg/mL Gramicidin D (Sigma G5002). Tight seals were held until sufficient access allowed injection of current and resolution of action potentials (typically 10–20 minutes). Ruptures of the perforated patch were apparent by a rapid drop in series resistance at which point the recordings were discontinued. Photo-stimulation of L6 *in vitro* consisted of either single 2 ms pulses or 40 Hz train of 2 ms pulses, or of 1s long ramps of light of increasing intensity as previously described[32]. Data were recorded with Multiclamp 700B amplifiers (Axon instruments) filtered at 2kHz and digitized with a Digidata1440A (Axon instruments) at 10kHz. Recordings were analyzed using custom made routines in Igor Pro (Wavemetrics). Charges represent the time integral of the synaptic current recorded during the first second of photo-stimulation. The stage was moved using a custom made plugin for ImageJ(NIH) to interface with ESP300 (Newport) via SerialPort (SerialIO). Drugs used: NBQX (Tocris 1044); CPP (Ascent Asc-159).

In vivo anesthetized recordings

Recordings were performed similarly to that previously described[22]. Animals were anesthetized with 5 mg/kg of chlorporthixene (i.p.) followed (5–10 minutes later) by 1.2 g/kg urethane (i.p). During surgery animals were given 0.5–1.0% isoflurane. Animals were placed onto a custom platform and their temperature maintained at 37 °C using a feedback-controlled heating pad (FHC). Whiskers and eyelashes contralateral to the recording side were trimmed and eyes covered with a thin, uniform layer of silcone oil to prevent drying. Protein expression was verified via transcranial epifluorescence of the exposed and PBS moistened skull using a Leica MZ10F microscope. Only animals showing expression over the entire extent of V1 were used for subsequent experiments. The entire dried skull was covered with black dental cement (Ortho-Jet powder (Lang Dental) mixed with black iron oxide) but for the previously outlined boundaries of V1 (~1.5–3.5 mm lateral to midline and −0.5 to 2.5 mm anterior to lambda suture). A headplate with a hole of ~2 mm diameter was mounted over V1 and a small region of skull (~300 × 750 μm) was thinned using a dental drill. Next we used sharpened fine forcesp (Dumont #55) to make a craniotomy just sufficiently large for inserting the probe. A drop of PBS placed in the well at the center of the headplate kept the exposed skull and craniotomy moist. A multichannel silicon probe

mounted on a micromanipulator (Luigs-Neumann) was slowly advanced into the brain to a depth of 800–1000 μm for linear probes and 200–700 μm for tetrode probes (see below) and recordings started at least 20 minutes after inserting the probe.

For dLGN recordings we made a circular craniotomy (~1.5 mm diamater) at 2.6 mm posterior and 2 mm lateral from the bregma suture. Robust visual responses and bursting activity characteristic of dLGN relay neurons were encountered at a depth between 2,400 and 3,100 μm[44] (Supplementary Fig. 7). For dual recording experiments (Fig. 3g,h and Fig. 5) we used a larger headplate so a craniotomy could be made both over the dLGN and V1.

Recordings were made with NeuroNexus 16 channel linear (a1×16-3mm-50-177) or tetrode (a2×2-tet-3mm-150-121) silicon probes. For recordings across cortical depth and in dLGN we used the linear configuration. The tetrode configuration was used to isolate a subset of cells in Fig. 2. Signals were amplified 1000x, band-pass filtered between 0.3 Hz and 5 kHz using an AM Systems 3500 amplifier and acquired at 32 kHz using a NIDAQ board (PCIe-6239) controlled with custom-written software in Matlab (Mathworks). For dual recording experiments we used two separate data acquisition setups (amplifier, NIDAQ board, and computer). Raw data was stored on a computer hard drive for offline analysis.

At the end of the recording session, animals were euthanized by administering 4% isoflorane and the brain quickly removed and fixed in 4% paraformaldehyde for histological analysis.

In vivo awake recordings

1–2 weeks prior to recording mice were implanted with a headplate for head-fixation. Mice were anesthetized with 2.5% isoflurane, the scalp removed, and a headplate fixed over V1 with black dental cement. The skull directly overlying V1 was covered with Kwik-Cast (WPI). Animals were injected subcutaneously with 0.1 mg/kg buprenorphine and allowed to recover in their home cage for at least 1 week before recording.

Several days prior to recording mice were familiarized to head-fixation within the recording setup. They were briefly anesthetized with isoflurane and the headplate clamped to a metal post but otherwise kept unrestrained and allowed to run in place on a plastic circular track (Fast-Trac from Bio-Serv; See Supplemental Fig. 6; the same circular track was present in the mice's cages where they were familiarized with its use). Mice grew accustomed to head-fixation over the course of one to three 15 minute sessions and ran naturally on the track, occasionally stopping to rest or groom.

On the day of recording, mice were anesthetized with 1.5–2% isoflurane, a small craniotomy made over V1, a drop of PBS placed in the well of the headplate clamped to a metal post, and the multichannel probe inserted into the craniotomy. After removal of isoflurane the mice regained consciousness and typically began running. Recordings did not start before 30 min. after the end of anesthesia. Awake recording sessions lasted between 1–2 hours. Mice typically spent ~60–80% their time running, while the rest of the time was spent resting or grooming. Data were not separated according to behavior. Every 30–60 minutes mice were given a few drops of a 5% glucose solution via a disposable pipette. For two mice we performed 2–3 recording sessions, which were made at least a day apart. Between sessions the craniotomy was covered with Kwik-Cast. A new craniotomy was made for each session.

Visual stimulation

Visual stimuli were generated in Matlab using the Psychophysics Toolbox[45] and were displayed on a gamma corrected LCD monitor (Dell 52 × 32.5 cm, 60 Hz refresh rate, mean luminance 50 cd/m^2) positioned 25 cm from the contralateral eye. The monitor was positioned for each experiment such that the multiunit receptive field was located

approximately in the center of the screen (the multiunit receptive field was determined by moving a localized drifting grating patch (~10°) around the screen). During the recording session full-field sinusoidal drifting gratings were used. All stimuli had a temporal frequency of 2 Hz and a spatial frequency of 0.04 cyles/degree. Gratings were randomly presented at 8–12 equally spaced directions, except for the experiments in Fig. 5 in which we only used 2 orthogonal grating directions (0 and 90°). The contrast of the stimulus was 100%, except for Fig. 5 in which we used 6 contrast levels (2, 4.4, 9.6, 21, 46, and 100%). A gray screen trial was interleaved with the drifting gratings. The duration of the visual stimulus was 1.5 s and the inter-trial interval was 3–6 s.

In vivo photo-stimulation

To photo-stimulate ChR2 we used a blue (470 nm) fiber-coupled LED (1 mm diameter, Doric Lenses) placed ~5–10 mm away from skull. Light from the LED spanned the entire area of V1. An opaque shield of black aluminum foil (Thor Labs) prevented LED light from reaching the contralateral eye. The LED was driven by the analog output from the NIDAQ board. The blue LED was presented at 5 intensities (approximately 3, 5, 7, 10.5, 20 mW measured at the tip of the fiber), but for a minority of experiments where we only presented the highest LED intensity. Trials were alternated between visual stimulus only and visual stimulus + LED. The strongest LED intensity also generated oscillations at gamma frequency, consistent with previous observations (Supplementary Fig. 2[32]). The preferred orientation photo-stimulated L6 cells remained unchanged yet their tuning curves became broader Supplementary Fig. 2).

To photo-stimulate Arch/NpHR3.0 we used an amber (590 nm) fiber-coupled LED (1 mm diameter, Doric Lenses) placed ~0.5 mm from skull. Because photo-suppression of L6 produced a transient decrease in spontaneous multiunit activity in L2–5 at the onset of LED illumination (see Supplemental Fig. 6) we turned on the amber LED 1.4 s before the visual stimulus began. Experiments were performed at the highest LED intensity (~20 mW measured at the tip of the fiber). As long as the suppresssion was not complete, the preferred orientation of photo-suppressed L6 cells remained unchanged (Supplementary Fig. 6).

In vivo data analysis

All in vivo data analysis was performed with custom software written in Matlab.

Multiunit analysis—Multiunit spiking activity was defined as all events (spikes) exceeding a threshold of 4 SD above the noise of the high-pass filtered (500 Hz) signal. Spikes were assigned a depth corresponding to the depth of the channel they were recorded from. Spikes recorded simultaneously on multiple channels were considered as a single event and attributed to the channel where they showed the largest amplitude. We determined the depth of each channel by considering the depth and the angle of the probe relative to the vertical axis of cortex. We assigned spikes to different layers according to the following depths (in μm): 100–350: L2/3; 350–450: L4; 450–650: L5; > 650: L6. Peri-stimulus time histograms (PSTHs) were composed of 50 ms bins. PSTHs of individual experiments were normalized to the first 500 ms of the visual stimulus (for ChR2 experiments) or to the entire visual stimulus (for Arch/ NpHR3.0 experiments) to generate average PSTHs. PSTHs for kinetic analysis (Fig. 3h) were composed of 3 ms bins and report the normalized difference in firing rates between control (average firing over a 50 ms window prior LED onset) and during LED illumination (average firing rate over a 100 ms window, 50 ms after LED onset). The onset of suppression was determined, for each experiment, as the time point at which the normalized response fell below 2 SD of the baseline.

The contrast response functions in dLGN and V1 report the normalized, baseline subtracted firing rates and were fitted with a hyperbolic ratio function:

$$r = r_{\max}\frac{c^n}{c^n + c_{50}^n}$$

where r is the response, c is the contrast of the visual stimulus, r_{max} is a fitted constant representing the response saturation level, n is fitting exponent that affects the shape of the curve, and c_{50} is the semi-saturation constant. The transfer function between the dLGN and V1 was fitted with a hyperbolic ratio function:

$$r_{V1} = r_{V1,\max}\frac{r_{dLGN}^n}{r_{dLGN}^n + r_{dLGN,50}^n}$$

where r_{V1} is the V1 response, $r_{V1,max}$ is a constant representing the V1 saturation level, r_{dLGN} is the dLGN response, n is a fitting exponent, and $r_{dLGN,50}$ is the semisaturation constant. The "cortico-thalamic (CT) component" was defined as the fraction of the total V1 suppression accounted for by this predicted response. The "intra-cortical component" was then defined as (1-CT component). We performed this analysis for 5 LED levels and averaged across experiments to produce the plot in Fig. 5f.

Single unit analysis—We isolated single units using spike sorting software provided by Hill, Mehta, and Kleinfeld[46]. For both the linear and tetrode probes we analyzed waveforms extracted from groups of 4 adjacent electrode sites. We high-pass filtered the raw signal at 500 Hz and then detected spiking events exceeding 4–5 SD of the noise. Spike waveforms were clustered using a k-means algorigthm. Following initial automated clustering, we used a graphical user interface to manually merge and split clusters. Unit isolation quality was assessed by considering refractory period violations and Fisher linear discriminant analysis. In agreement with previous studies we could classify waveforms as regular spiking (RS) or fast spiking (FS) putative inhibitory neurons. In our dataset there was a clear bimodal distribution of trough-to-peak times (a threshold of 0.4 ms was used to divide FS from RS units). All units were assigned a depth according the channel they were detected on, and units were assigned to layers based on the depth divisions given above for the multiunit activity.

For each unit we computed the visual response as the mean spike rate occurring over the time window in which both the LED and visual stimulus were present. Thus, for the L6 photo-stimulation experiments this typically corresponded to a 500 ms window placed in the center of the visual response, and for the L6 photo-suppression experiments this window encompassed the entire 1.5 s visual stimulus. For all analysis except the orientation tuning analyis in Fig. 2, we averaged responses over all stimulus conditions. Following recent studies[47, 48] of orientation tuning we computed an orientation selectivity index (OSI) as:

$$OSI = \frac{\sqrt{(\sum r_k \sin(2\theta_k))^2 + (\sum r_k \cos(2\theta_k))^2}}{\sum r_k}$$

where r_k is the response to the kth direction given by θ_k. We determined an OSI for each unit with and without photo-stimulation/suppression of L6. We determined the preferred

orientation and tuning width by first fitting the average responses of each unit with a sum of 2 gaussians:

$$r=r_0+r_p e^{-(\theta-\theta_p)^2/(2\sigma^2)}+r_{p+180}e^{-(\theta-\theta_p-180)^2/(2\sigma^2)}$$

where r_0 is a constant offset, r_p is the response at the preferred orientation, r_{p+180} is response 180° away from preferred direction, θ is the stimulus direction, θ_p is the preferred orientation, and σ is the tuning width. The two gaussians were forced to peak 180° apart and to have the same width, but could have different amplitudes. Control and photo-stimulution/suppression conditions were fit separately. To generate the average population tuning curve we first circularly shifted the stimulus direction of each unit such that the maximal response occurred at 0°. We then normalized the responses to this peak response and averaged all normalized tuning curves together. We fit the control population average tuning curve with a sum of 2 gaussians. The curve for the photo-stimulation/suppression population average was produced by scaling the control curve by the slope (gain factor) of the linear fit shown in either Fig. 2e or 2j.

All results are presented as mean±sem unless otherwise noted. We used paired *t*-tests to assess statistical significance unless otherwise noted.

Histology

Triple transgenic mice (Ntsr1-Cre, floxed-tdTomato, and Gad67-GFP) were anesthetized with ketamine and xylazine (100mg/kg and 10mg/kg, respectively) and perfused with cold sucrose (see above) and then PFA (4% in PBS). After 24hr incubation in PFA, slices were cut into 50 μm sections and immunostained as described previously[49]. Antibodies used were: mouse anti-NeuN (1:400; Millipore MAB377); chicken anti-GFP(1:1000; Aves Labs, Inc. GFP-1020) goat anti-chicken AF488 (1:1000; Invitrogen A11039) and goat anti-mouse AF633(1:1000; Invitrogen A21050). Slices were mounted in Vectashield with Dapi (Vector Labs, H1500). Images were single confocal sections taken on an Olympus FV1000. Layer borders were identified by changes in cell density. Cell counts were done using standard stereological techniques. Biocytin fills and neural reconstructions were done as previously described[50].

Supplementary Material

Refer to Web version on PubMed Central for supplementary material.

Acknowledgments

We are grateful to M. Carandini, J. Isaacson and the members of the Scanziani and Isaacson labs for helpful discussions of this project; to J. Isaacson, R. Malinow, and T. Komiyama for providing feedback on the manuscript; to P. Abelkop for histological help and neonatal viral injections; to J. Evora for mouse colony support and genotyping; to B. Atallah for sharing the technique for silencing the cortex by photo-stimulation of PV neurons and for help with the in vivo recording setup; to W. Bruns for help coding analysis software. S.R.O. and H.A. were supported by postdoctoral fellowships from the Helen Hay Whitney Foundation. M.S. is an investigator of the Howard Hughes Medical Institute. This work was also supported NIH grant RC1 NS069010 and by the Gatsby Charitable Foundation.

References

1. Lorente de No, R. Physiology of the nervous system. JFF, editor. Oxford University Press; Oxford: 1943. p. 274-301.

2. Douglas RJ, Martin KA. Neuronal circuits of the neocortex. Annu Rev Neurosci. 2004; 27:419–51. [PubMed: 15217339]
3. Lefort S, Tomm C, Floyd Sarria JC, Petersen CC. The excitatory neuronal network of the C2 barrel column in mouse primary somatosensory cortex. Neuron. 2009; 61:301–16. [PubMed: 19186171]
4. Thomson AM, Bannister AP. Interlaminar connections in the neocortex. Cereb Cortex. 2003; 13:5–14. [PubMed: 12466210]
5. Callaway EM. Local circuits in primary visual cortex of the macaque monkey. Annu Rev Neurosci. 1998; 21:47–74. [PubMed: 9530491]
6. Dantzker JL, Callaway EM. Laminar sources of synaptic input to cortical inhibitory interneurons and pyramidal neurons. Nat Neurosci. 2000; 3:701–7. [PubMed: 10862703]
7. Thomson AM. Neocortical layer 6, a review. Front Neuroanat. 2010; 4:13. [PubMed: 20556241]
8. Bourassa J, Deschenes M. Corticothalamic projections from the primary visual cortex in rats: a single fiber study using biocytin as an anterograde tracer. Neuroscience. 1995; 66:253–63. [PubMed: 7477870]
9. Binzegger T, Douglas RJ, Martin KA. Stereotypical bouton clustering of individual neurons in cat primary visual cortex. J Neurosci. 2007; 27:12242–54. [PubMed: 17989290]
10. Zhang ZW, Deschenes M. Intracortical axonal projections of lamina VI cells of the primary somatosensory cortex in the rat: a single-cell labeling study. J Neurosci. 1997; 17:6365–79. [PubMed: 9236245]
11. Jones, EG. Thalamus. University of Cambridge; Cambridge: 2007.
12. Guillery RW, Sherman SM. Thalamic relay functions and their role in corticocortical communication: generalizations from the visual system. Neuron. 2002; 33:163–75. [PubMed: 11804565]
13. Sillito AM, Jones HE. Corticothalamic interactions in the transfer of visual information. Philos Trans R Soc Lond B Biol Sci. 2002; 357:1739–52. [PubMed: 12626008]
14. Briggs F, Usrey WM. Emerging views of corticothalamic function. Curr Opin Neurobiol. 2008; 18:403–7. [PubMed: 18805486]
15. Cudeiro J, Sillito AM. Looking back: corticothalamic feedback and early visual processing. Trends Neurosci. 2006; 29:298–306. [PubMed: 16712965]
16. Sillito AM, Cudeiro J, Jones HE. Always returning: feedback and sensory processing in visual cortex and thalamus. Trends Neurosci. 2006; 29:307–16. [PubMed: 16713635]
17. Bolz J, Gilbert CD. Generation of end-inhibition in the visual cortex via interlaminar connections. Nature. 1986; 320:362–5. [PubMed: 3960119]
18. Grieve KL, Sillito AM. A re-appraisal of the role of layer VI of the visual cortex in the generation of cortical end inhibition. Exp Brain Res. 1991; 87:521–9. [PubMed: 1783022]
19. Gong S, et al. Targeting Cre recombinase to specific neuron populations with bacterial artificial chromosome constructs. J Neurosci. 2007; 27:9817–23. [PubMed: 17855595]
20. Nagel G, et al. Channelrhodopsin-2, a directly light-gated cation-selective membrane channel. Proc Natl Acad Sci U S A. 2003; 100:13940–5. [PubMed: 14615590]
21. Boyden ES, Zhang F, Bamberg E, Nagel G, Deisseroth K. Millisecond-timescale, genetically targeted optical control of neural activity. Nat Neurosci. 2005; 8:1263–8. [PubMed: 16116447]
22. Niell CM, Stryker MP. Highly selective receptive fields in mouse visual cortex. J Neurosci. 2008; 28:7520–36. [PubMed: 18650330]
23. Hubel DH, Wiesel TN. Receptive fields, binocular interaction and functional architecture in the cat's visual cortex. J Physiol. 1962; 160:106–54. [PubMed: 14449617]
24. Chow BY, et al. High-performance genetically targetable optical neural silencing by light-driven proton pumps. Nature. 2011; 463:98–102. [PubMed: 20054397]
25. Gradinaru V, et al. Molecular and cellular approaches for diversifying and extending optogenetics. Cell. 2010; 141:154–65. [PubMed: 20303157]
26. Rafols JA, Valverde F. The structure of the dorsal lateral geniculate nucleus in the mouse. A Golgi and electron microscopic study. J Comp Neurol. 1973; 150:303–32. [PubMed: 4124620]
27. Salinas E, Thier P. Gain modulation: a major computational principle of the central nervous system. Neuron. 2000; 27:15–21. [PubMed: 10939327]

28. Brotchie PR, Andersen RA, Snyder LH, Goodman SJ. Head position signals used by parietal neurons to encode locations of visual stimuli. Nature. 1995; 375:232–5. [PubMed: 7746323]
29. Treue S, Martinez Trujillo JC. Feature-based attention influences motion processing gain in macaque visual cortex. Nature. 1999; 399:575–9. [PubMed: 10376597]
30. McAdams CJ, Maunsell JH. Effects of attention on orientation-tuning functions of single neurons in macaque cortical area V4. J Neurosci. 1999; 19:431–41. [PubMed: 9870971]
31. Silver RA, Lubke J, Sakmann B, Feldmeyer D. High-probability uniquantal transmission at excitatory synapses in barrel cortex. Science. 2003; 302:1981–4. [PubMed: 14671309]
32. Adesnik H, Scanziani M. Lateral competition for cortical space by layer-specific horizontal circuits. Nature. 2010; 464:1155–60. [PubMed: 20414303]
33. Markram H, et al. Interneurons of the neocortical inhibitory system. Nat Rev Neurosci. 2004; 5:793–807. [PubMed: 15378039]
34. Ascoli GA, et al. Petilla terminology: nomenclature of features of GABAergic interneurons of the cerebral cortex. Nat Rev Neurosci. 2008; 9:557–68. [PubMed: 18568015]
35. Chance FS, Abbott LF, Reyes AD. Gain modulation from background synaptic input. Neuron. 2002; 35:773–82. [PubMed: 12194875]
36. Shadlen MN, Newsome WT. The variable discharge of cortical neurons: implications for connectivity, computation, and information coding. J Neurosci. 1998; 18:3870–96. [PubMed: 9570816]
37. Murphy BK, Miller KD. Multiplicative gain changes are induced by excitation or inhibition alone. J Neurosci. 2003; 23:10040–51. [PubMed: 14602818]
38. Andolina IM, Jones HE, Wang W, Sillito AM. Corticothalamic feedback enhances stimulus response precision in the visual system. Proc Natl Acad Sci U S A. 2007; 104:1685–90. [PubMed: 17237220]
39. Wang W, Jones HE, Andolina IM, Salt TE, Sillito AM. Functional alignment of feedback effects from visual cortex to thalamus. Nat Neurosci. 2006; 9:1330–6. [PubMed: 16980966]
40. Worgotter F, Nelle E, Li B, Funke K. The influence of corticofugal feedback on the temporal structure of visual responses of cat thalamic relay cells. J Physiol. 1998; 509 (Pt 3):797–815. [PubMed: 9596801]
41. McClurkin JW, Marrocco RT. Visual cortical input alters spatial tuning in monkey lateral geniculate nucleus cells. J Physiol. 1984; 348:135–52. [PubMed: 6716281]
42. Murphy PC, Duckett SG, Sillito AM. Feedback connections to the lateral geniculate nucleus and cortical response properties. Science. 1999; 286:1552–4. [PubMed: 10567260]
43. Casagrande, VA.; KJH. The afferent, intrinsic and efferent connections of primary visual cortex in primates. Rockland, P., editor. 1994.
44. Grubb MS, Thompson ID. Quantitative characterization of visual response properties in the mouse dorsal lateral geniculate nucleus. J Neurophysiol. 2003; 90:3594–607. [PubMed: 12944530]
45. Brainard DH. The Psychophysics Toolbox. Spat Vis. 1997; 10:433–6. [PubMed: 9176952]
46. Fee MS, Mitra PP, Kleinfeld D. Automatic sorting of multiple unit neuronal signals in the presence of anisotropic and non-Gaussian variability. J Neurosci Methods. 1996; 69:175–88. [PubMed: 8946321]
47. Kerlin AM, Andermann ML, Berezovskii VK, Reid RC. Broadly tuned response properties of diverse inhibitory neuron subtypes in mouse visual cortex. Neuron. 2010; 67:858–71. [PubMed: 20826316]
48. Ringach DL, Shapley RM, Hawken MJ. Orientation selectivity in macaque V1: diversity and laminar dependence. J Neurosci. 2002; 22:5639–51. [PubMed: 12097515]
49. Bortone D, Polleux F. KCC2 expression promotes the termination of cortical interneuron migration in a voltage-sensitive calcium-dependent manner. Neuron. 2009; 62:53–71. [PubMed: 19376067]
50. Bagnall MW, Hull C, Bushong EA, Ellisman MH, Scanziani M. Multiple Clusters of Release Sites Formed by Individual Thalamic Afferents onto Cortical Interneurons Ensure Reliable Transmission. Neuron. 2011; 71:180–94. [PubMed: 21745647]

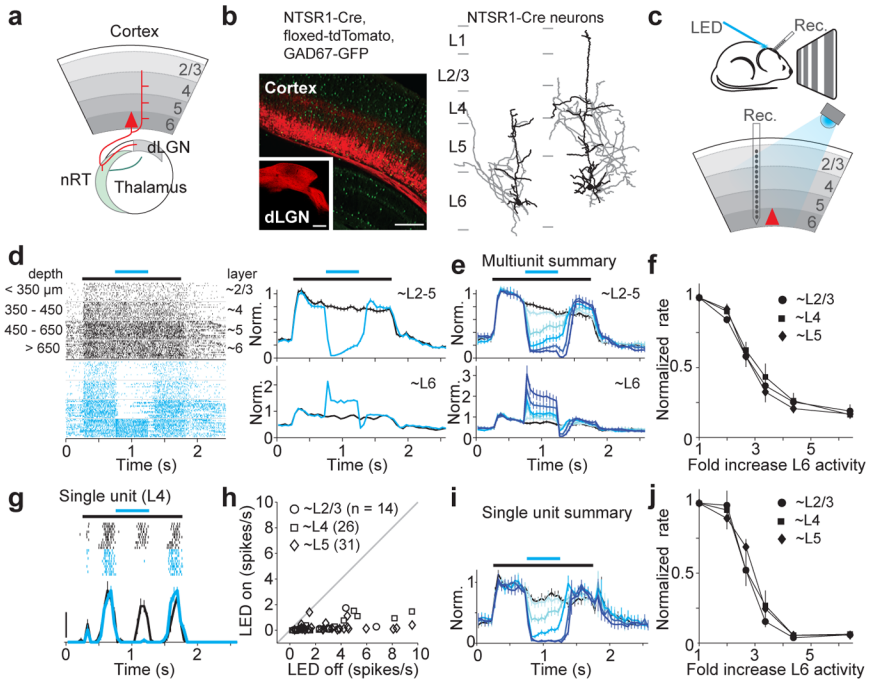

Figure 1. Photo-stimulation of L6 suppresses visual responses in the other layers

a. Schematic of L6 projections.

b. Left, coronal section of V1 from NTSR1-Cre, floxed-tdTomato, GAD67-GFP mouse. Inset, L6 projection to dLGN (V1 of NTSR1-Cre mouse was injected with floxed-tdTomato virus). Right, The two types of L6 neurons labeled by the NTSR1-Cre line. Dendrites: black; axons: gray.

c. Schematic of setup.

d. Cortical visual responses with (blue) and without (black) L6 photo-stimulation. Left, raster plot of multiunit activity grouped by depth. Control and photo-stimulation trials were interleaved but are separated here for clarity. Black bar: visual stimulus (1.5 s); blue bar: LED illumination (0.5 s). Right, normalized PSTH; top: upper layers; bottom: L6.

e. Summary (n = 6 experiments). Control in black and increasing LED intensities in darker blues.

f. Suppression of multiunit activity with increasing L6 activity.

g. Visual response of single L4 unit with (blue) and without (black) L6 photo-stimulation. Scale bar, 20 spikes/s.

h. Response of each regular spiking unit with and without strong photo-stimulation of L6.

i. Average normalized PSTH (n = 47 units tested with 5 LED intensities). Colors as in (e).

j. Suppression of single unit activity.

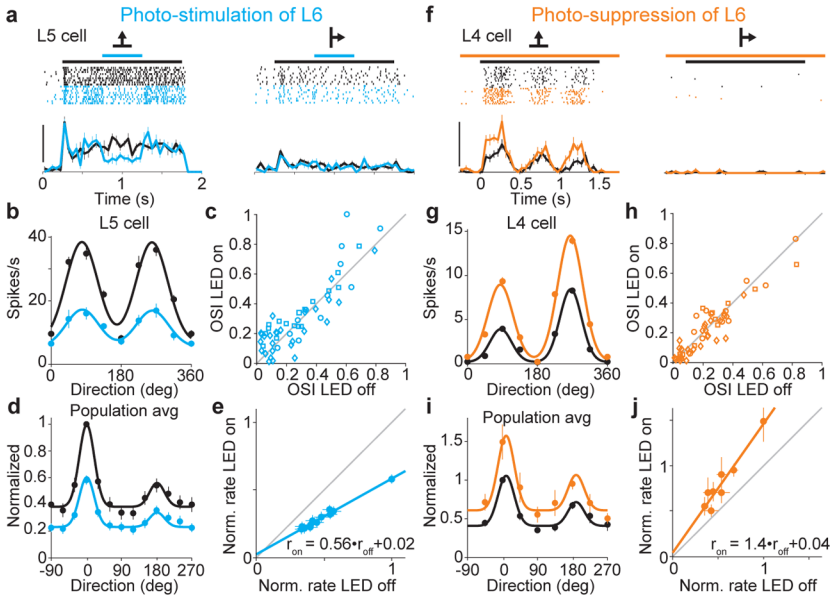

Figure 2. L6 bidirectionally modulates gain of visual responses without altering tuning

a. Visual responses of L5 neuron (2 of 8 tested directions) with (blue) and without (black) L6 photo-stimulation. Scale bar, 40 spikes/s.

b. Tuning curves for neuron in (a).

c. Orientation selectivity index (OSI) for each neuron with and without photo-stimulation of L6.

d. Population tuning curve with (blue) and without (black) L6 photo-stimulation (n = 55). Black curve: fit using sum of two gaussians. Blue curve is black curve scaled by slope of linear fit in (e).

e. Control response plotted against response with L6 photo-stimulation (data from c). Linear fit (blue; $r^2 = 0.98$).

f. Visual response of L4 neuron with (orange) and without (black) L6 photo-suppression. Scale bar, 50 spikes/s.

g. Tuning curves for neuron in (f).

h. OSI for each isolated unit with and without photo-suppression of L6.

i. Population tuning curves with and without L6 photo-suppression (n = 52). Black curve: fit using sum of two gaussians. Orange curve is black curve scaled by slope of linear fit in (j).

j. Control response plotted against response with L6 photo-stimulation (data from i). Linear fit (orange; $r^2 = 0.92$).

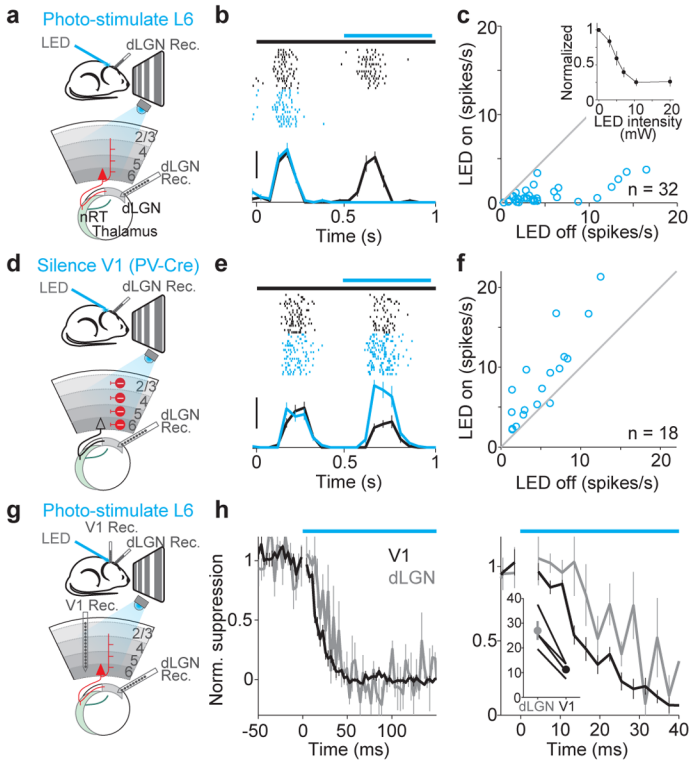

Figure 3. Photo-stimulation of L6 suppresses cortex faster than it suppresses dLGN

a. Schematic of setup.

b. Visual response of dLGN unit with (blue) and without (black) L6 photo-stimulation Scale bar, 20 spikes/s.

c. Average response of each dLGN unit with and without L6 photo-stimulation. Inset, monotonic suppression of dLGN.

d. Schematic of setup for silencing V1 by photo-stimulation of PV inhibitory neurons.

e. Visual response of dLGN unit with and without photo-silencing of V1. Scale bar, 30 spikes/s

f. Average response of each dLGN unit with and without cortical silencing.

g. Schematic of setup.

h. Left, time-course of L6-mediated suppression of dLGN (gray) and V1 (black) (n = 4). Bin size: 3 ms. Right, same data on expanded timescale. The first bin at LED onset was blanked to remove LED-induced artifact. Inset, time to suppression exceeding 2 SDs from baseline activity in dLGN and V1 (y-axis: ms) for four experiments (p = 0.012).

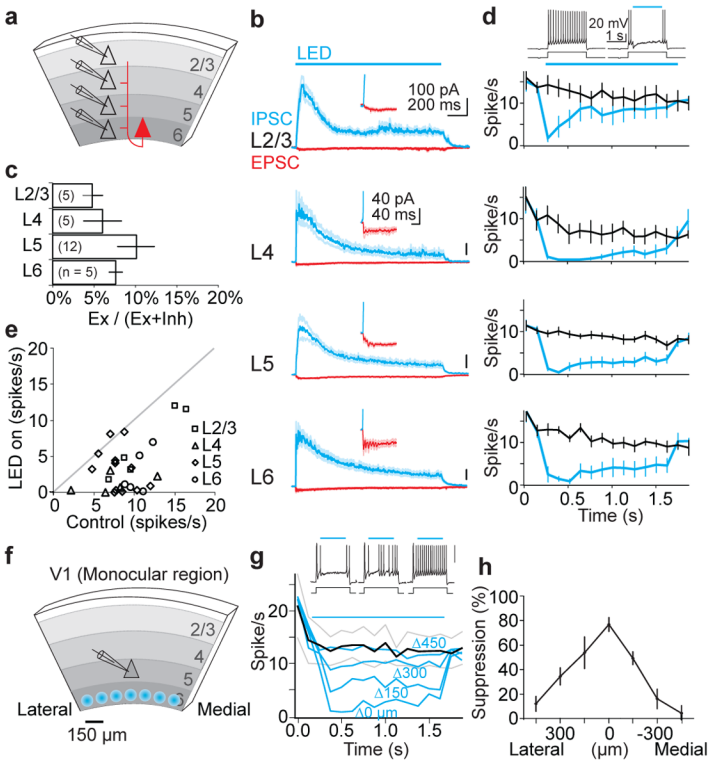

Figure 4. Photo-stimulation of L6 recruits intra-cortical synaptic inhibition

a. Schematic of in vitro setup.

b. Average IPSCs (blue) and EPSCs (red) recorded in pyramidal cells during photo-stimulation of L6. Synaptic currents are averages of n = 5–12 cells. Inset, onset of EPSC.

c. Histogram of excitatory charge as a percentage of total charge.

d. Top traces: perforated patch recording from L5 pyramidal cell in response to depolarizing current injection with (right) and without (left) L6 photo-stimulation. Bottom graphs: spike rate with and without L6 photo-stimulation.

e. Average spike rate in control versus spike rate with L6 photo-stimulation for each cell.

f. Schematic of setup for focal photo-stimulation.

g. Top traces: spiking of L5 pyramidal cell to depolarizing current injection with focal photo-stimulation of L6 at three progressively more distant positions (left to right). Bottom graph: spike rate in control (black) and with focal photo-stimulation of L6 (blue) (n = 4). Delta indicates medial/lateral distance from radial axis through recording site.

h. Percentage of spike suppression plotted against horizontal displacement.

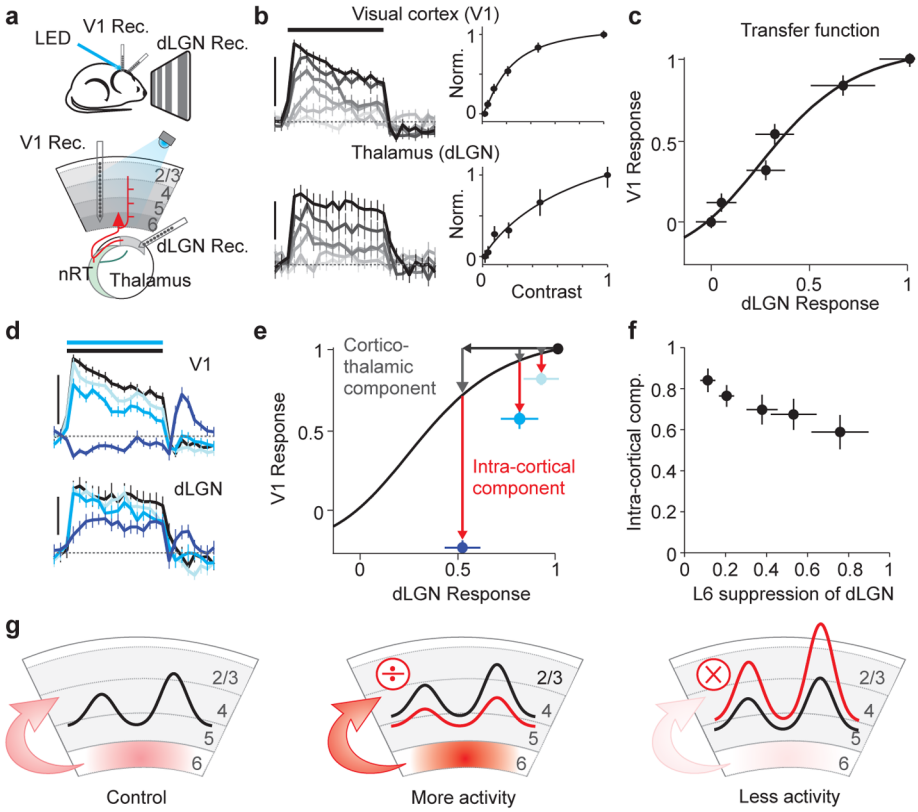

Figure 5. L6 suppresses upper layers largely through intra-cortical circuits

a. Schematic of setup.

b. Simultaneously recorded multiunit responses to increasing contrasts (light to dark) in V1 (top) and dLGN (bottom). All spikes recorded above L6 (≤650 μm) were included in V1 multiunit activity. Scale bar: V1: 200 spikes/s; LGN: 100 spikes/s. Dotted line: baseline activity. Right, contrast response functions.

c. dLGN-V1 transfer function derived by plotting normalized response in V1 versus dLGN (from b). Fit: hyperbolic ratio function.

d. Simultaneously recorded multiunit responses to maximal contrasts in V1 (top) and dLGN (bottom) in control (black) or while photo-stimulating L6 with increasing LED intensities (progressively darker blue). Same experiment as in b and c. Scale bars: as in (b).

e. V1 versus dLGN response to maximal contrast under control condition (black data point) or during three progressively stronger photo-stimulation of L6 (light, medium and dark blue; data from d). V1 responses are suppressed more than predicted by transfer function (red arrows) even for photo-stimulations that reduce dLGN activity only ~ 10% (light blue).

f. Average intra-cortical component of suppression as function of suppression of dLGN (n = 5 experiments). Intra-cortical component (red arrow in e) is quantified as fraction of total V1 suppression (gray arrow + red arrow in e).

g. Schematic of main finding.